AFRL-RY-WP-TR-2020-0003

OPEN CIRCUIT VOLTAGE PHOTODETECTOR (VocP) INFRARED IMAGER

Sanjay Krishna, Waleed Khalil, T.J. Ronningen, Rudy Fink, Roman "Gus" Fragasse, Shane Smith, Zahra Tahgipour, Teressa Specht, and Phillip Van Hooser
The Ohio State University
Department of Electrical and Computer Engineering

Earl Fuller
SK Infrared

Ramy Tantawy
Sense IC

MARCH 2020
Final Report

STINFO COPY

AIR FORCE RESEARCH LABORATORY
SENSORS DIRECTORATE
WRIGHT-PATTERSON AIR FORCE BASE, OH 45433-7320
AIR FORCE MATERIEL COMMAND
UNITED STATES AIR FORCE

NOTICE AND SIGNATURE PAGE

This report is the result of contracted fundamental research deemed exempt from public affairs security and policy review in accordance with The Under Secretary of Defense memorandum dated 24 May 2010 and AFRL/DSO policy clarification email dated 13 January 2020. This report is available to the general public, including foreign nationals.

Copies may be obtained from the Defense Technical Information Center (DTIC) (http://www.dtic.mil).

AFRL-RY-WP-TR-2020-0003 HAS BEEN REVIEWED AND IS APPROVED FOR PUBLICATION IN ACCORDANCE WITH ASSIGNED DISTRIBUTION STATEMENT.

ARIYAWANSA.G AMINI.140265632 4
Digitally signed by ARIYAWANSA.GAMINI.14026 56324
Date: 2020.02.26 12:44:32 -05'00'

*GAMINI ARIYAWANSA, Program Manager
Electro-Optic/Infrared Components Branch
Aerospace Components & Subsystems Division

ARNOLD.FRED .E.1230167598
Digitally signed by ARNOLD.FRED.E.123016759 8
Date: 2020.02.26 15:41:40 -05'00'

FRED E. ARNOLD, Chief
Electro-Optic/Infrared Components Branch
Aerospace Components & Subsystems Division

BROOKS.ADAM .L.1270115205
Digitally signed by BROOKS.ADAM.L.1270115205
Date: 2020.02.27 18:05:42 -05'00'

ADAM L. BROOKS, Lt Col, USAF
Deputy
Aerospace Component & Subsystems Division
Sensors Directorate

This report is published in the interest of scientific and technical information exchange, and its publication does not constitute the Government's approval or disapproval of its ideas or findings.

*Disseminated copies will show "//Signature//" stamped or typed above the signature blocks.

REPORT DOCUMENTATION PAGE

1. REPORT DATE *(DD-MM-YY)*	2. REPORT TYPE	3. DATES COVERED *(From - To)*
March 2020	Final	9 October 2018 – 9 October 2019

4. TITLE AND SUBTITLE	5a. CONTRACT NUMBER
OPEN CIRCUIT VOLTAGE PHOTODETECTOR (VocP) INFRARED IMAGER	FA8650-19-1-7913
	5b. GRANT NUMBER
	5c. PROGRAM ELEMENT NUMBER 62716E

6. AUTHOR(S)	5d. PROJECT NUMBER
Sanjay Krishna, Waleed Khalil, T.J. Ronningen, Rudy Fink, Roman "Gus" Fragasse, Shane Smith, Zahra Tahgipour, Teressa Specht, and Phillip Van Hooser (The Ohio State University, Department of Electrical and Computer Engineering) Earl Fuller (SK Infrared) Ramy Tantawy (Sense IC)	N/A
	5e. TASK NUMBER N/A
	5f. WORK UNIT NUMBER Y1WC

7. PERFORMING ORGANIZATION NAME(S) AND ADDRESS(ES)		8. PERFORMING ORGANIZATION REPORT NUMBER
The Ohio State University Department of Electrical and Computer Engineering 1960 Kenny Road Columbus, OH 43210-1016	SK Infrared Sense IC	

9. SPONSORING/MONITORING AGENCY NAME(S) AND ADDRESS(ES)		10. SPONSORING/MONITORING AGENCY ACRONYM(S)
Air Force Research Laboratory Sensors Directorate Wright-Patterson Air Force Base, OH 45433-7320 Air Force Materiel Command United States Air Force	Defense Advanced Research Projects Agency DARPA/MTO 675 North Randolph Street Arlington, VA 22203	AFRL/RYDH
		11. SPONSORING/MONITORING AGENCY REPORT NUMBER(S) AFRL-RY-WP-TR-2020-0003

12. DISTRIBUTION/AVAILABILITY STATEMENT
Approved for public release; distribution is unlimited.

13. SUPPLEMENTARY NOTES
This report is the result of contracted fundamental research deemed exempt from public affairs security and policy review in accordance with The Under Secretary of Defense memorandum dated 24 May 2010 and AFRL/DSO policy clarification email dated 13 January 2020. This material is based on research sponsored by Air Force Research Lab (AFRL) and the Defense Advanced Research Projects Agency (DARPA) under agreement number FA8650-19-1-7913. The U.S. Government is authorized to reproduce and distribute reprints for Governmental purposes notwithstanding any copyright notation thereon. The views and conclusions contained herein are those of the authors and should not be interpreted as necessarily representing the official policies or endorsements, either expressed or implied, of AFRL and DARPA or the U.S. Government. Report contains color.

14. ABSTRACT
In this project, the VocP team (Ohio State University and SK Infrared) demonstrated the performance of the Open Circuit Voltage Photodetector (VocP) pixel with two photovoltaic materials. The team has demonstrated the feasibility of implementing a VocP detector by operating a photodetector in an open-circuit voltage configuration and using it to control the gate-source voltage of a field effect transistor (FET). The team developed two experimental platforms for characterizing this approach and also made comparison measurements to a more traditional photodetector configuration. A model of the detector system was developed that accurately predicts the signal and noise performance of a VocP detector and enables further design work.

15. SUBJECT TERMS
Circuit Voltage, Photodetector, Infrared, Field Effect Transistor

16. SECURITY CLASSIFICATION OF:			17. LIMITATION OF ABSTRACT:	18. NUMBER OF PAGES	19a. NAME OF RESPONSIBLE PERSON (Monitor)
a. REPORT Unclassified	**b. ABSTRACT** Unclassified	**c. THIS PAGE** Unclassified	SAR	40	Gamini Ariyawansa **19b. TELEPHONE NUMBER** *(Include Area Code)* N/A

Table of Contents

List of Figures

List of Tables

LIST OF CONTRIBUTORS

Principal Investigators

Sanjay Krishna Professor and George R. Smith Chair in Engineering
Department of Electrical and Computer Engineering
The Ohio State University

Waleed Khalil Associate Professor
ElectroScience Laboratory
The Ohio State University

Earl Fuller, CEO, SK Infrared

Project Manager

TJ Ronningen, Research Scientist
Department of Electrical and Computer Engineering
The Ohio State University

Ohio State University Researchers

Rudy Fink, Graduate Research Assistant, Department of Electrical and Computer Engineering
Roman "Gus" Fragasse, Graduate Research Assistant, ElectroScience Laboratory
Shane Smith, Research Scientist, ElectroScience Laboratory
Zahra Tahgipour, Postdoctoral Researcher, Department of Electrical and Computer Engineering
Teressa Specht, Graduate Research Assistant, Department of Electrical and Computer Engineering
Phillip Van Hooser, Undergraduate Researcher, ElectroScience Laboratory

Sense IC Consultant

Ramy Tantawy, Founder, Sense IC

1. EXECUTIVE SUMMARY

In this project, the VocP team (Ohio State University and SK Infrared) demonstrated the performance of the Open Circuit Voltage Photodetector (VocP) pixel with two photovoltaic materials. For both of these materials, the team completed a side-by-side comparison of a more traditional, direct photocurrent, implementation with the VocP implementation and found (Figure 1) that the signal-to-noise ratio (SNR) of the VocP. While the measured noise equivalent power (NEP) of the VocP mode is not superior, it is within an order of magnitude of the photodiode mode, which holds the promise of being closed with identified design improvements. The laboratory measurements were compared with the team's system model and provided confirmation of that model's accuracy. The verified model enables us to make design decisions and more confident predictions of detector performance.
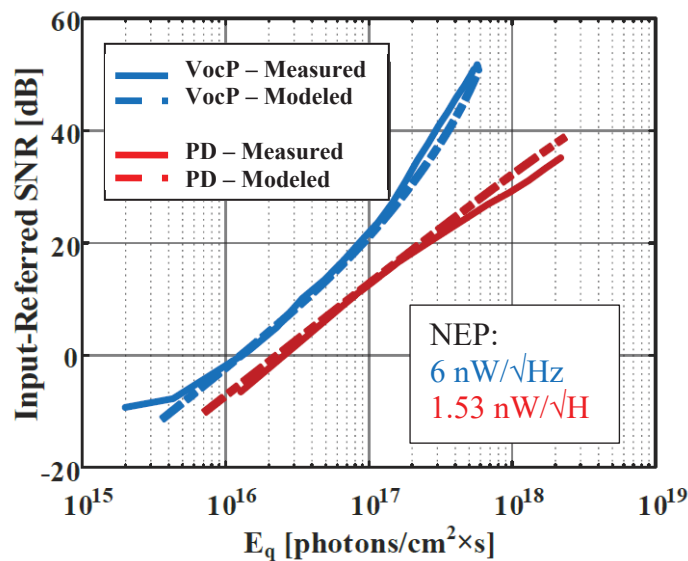
Figure 1: Measured and Modeled SNR vs. Photon Irradiance for both the Conventional PD and the VocP Pixels using the H300 Photodetector at Room Temperature
(Repeated as Figure 16)

The team has demonstrated the feasibility of implementing a VocP detector by operating a photodetector in an open-circuit voltage configuration and using it to control the gate-source voltage of a field effect transistor (FET). The team designed and implemented a custom readout integrated circuit (ROIC) designed for the VocP detection approach. The team developed two experimental platforms for characterizing this approach and also made comparison measurements to a more traditional configuration. The team developed a model of the detector system that accurately predicts the signal and noise performance of a VocP detector and enables further design work. The team's experimental and theoretical assessments identified the following advantages for a VocP detector:

- Pixel size reduction without a signal penalty and with a smaller noise penalty than a traditional photocurrent approach

Approved for public release; distribution is unlimited.

- Predicted NEP improvement by operation in VocP configuration over a traditional photocurrent configuration
- A reduction in the size of the ROIC integration capacitors, by several orders of magnitude, due to the reduction in the baseline, dark photocurrent
- The possibility of sensitive, high-speed imaging with these smaller capacitors
- A reduction in ROIC power demands by not applying a bias voltage to the photodiodes

2. PROJECT BACKGROUND

Ohio State University (OSU) and SK Infrared have developed a novel photodetector concept called the Open Circuit Voltage Photodetector (VocP). The VocP is a new approach to photon detection that uses the photosensitive material to generate an open circuit voltage (V_{OC}) and control the "photocurrent" through a transistor. The current flowing through the transistor is determined by V_{OC}, is proportional to the radiant power, and is monitored instead of the photodiode's current. The VocP is predicted to provide three advantages for infrared detection over a standard photocurrent implementation:

1. The VocP has a superior sensitivity as the pixel size shrinks because V_{OC} and the VocP signal are independent of pixel size. The VocP photocurrent remains constant as the pixel size decreases, but a standard photodiode's photocurrent decreases proportional to area [1]. If this superior sensitivity is not countermanded by an increased noise, then the VocP will also provide a superior NEP and detectivity.
2. The VocP has a large dynamic range because V_{OC} increases logarithmically with incident irradiance, but the signal, the photocurrent through the transistor, increases linearly. This increases the dynamic range of a VocP pixel by several orders of magnitude (o.o.m.) over a standard photodiode.
3. The VocP is designed for compatibility with the latest advances in commercial, visible image sensors, and its ROIC could have a cost and performance advantage over other infrared focal plane arrays (FPAs).

Based on these combined benefits, we assessed if VocP can provide superior performance over a conventional infrared photodetector (PD) approach in the dimensions of operating temperature, high speed detection, ROIC power consumption, and detectivity.

A VocP pixel is illustrated in Figure 2 in comparison to a PD circuit that monitors the photocurrent through the PD. The VocP detector is a parallel combination of photosensitive diodes (between 1 and n) connected to the gate of a FET. In Figure 2c, this is illustrated as the combination of a diode and FET M1. Due to the high impedance of the FET gate terminal, the VocP diode(s) are effectively loaded by an open circuit, no current flows through the diodes, and a V_{OC} is established that depends upon the incident irradiance. In Figure 2b, removing M1 makes the pixel a conventional PD configuration. In Figure 2a, the remainder of the ROIC pixel unit cell can be the same. However, as developed further below, optimizing the two approaches leads to differences in the integration capacitor (C_{INT}) that have circuit and performance consequences. The signal current in the PD case is several orders of magnitude higher than in the VocP case, and C_{INT} has to be selected accordingly. This difference is magnified at high operating temperatures (HOT) where C_{INT} has to be sized to account for the dark current in the PD case.
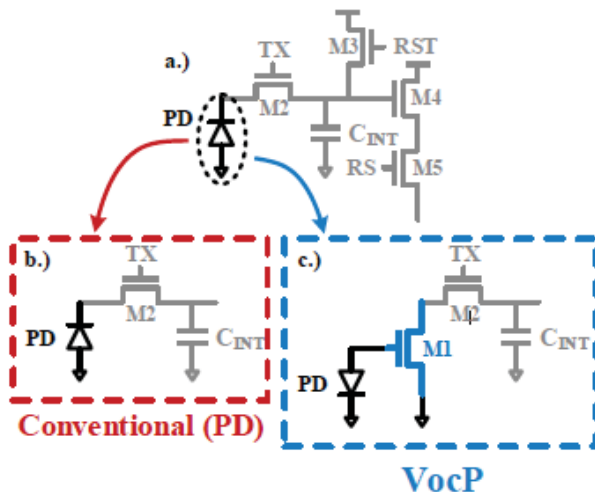
Figure 2: (a) Pixel Unit Cell compatible with both (b) Conventional PD Configuration that directly injects Current and (c) VocP Configuration with Current modulated through the M1 FET

Prior to this project, we demonstrated the concept of the VocP approach using discrete diodes and transistors. We developed an initial signal and noise model for the circuit that has been refined during this project. That initial model was used to set performance targets for discrete, custom components and for the integrated VocP pixel.

Approved for public release; distribution is unlimited.

3. PROJECT TECHNICAL OBJECTIVES

Under this Defense Advanced Research Projects Agency (DARPA) project, we aimed to demonstrate the potential of the VocP and reduce the risk for commercial implementation by:

1. Fabricating a mid-wave infrared (MWIR) photovoltaic diode for integration into a VocP detector
2. Producing a pixel unit cell of a VocP ROIC for integration into a VocP detector
3. Integrating and characterizing a VocP detector to demonstrate its performance and assess the accuracy of our VocP model

Table 1 specifies quantitative performance targets set for the two components and the integrated detector. Photovoltaic detector and pixel unit cell components that meet these targets were predicted to also meet the VocP pixel targets. We targeted meeting the Phase I performance targets within this project.

Table 1. Performance Targets for two Components and the Integrated Pixel Detector

COMPONENT	CHARACTERISTIC	PHASE I	PHASE II	PHASE III
PHOTOVOLTAIC	Peak response wavelength (λ_{Peak})		Between 3-5 µm	
PHOTOVOLTAIC	Responsivity at λ_{Peak}	≥ 0.1 A/W	≥ 0.5 A/W	≥ 1.0 A/W
PHOTOVOLTAIC	Dark current density at −5 mV	≤ 1 A/cm^2	≤ 0.1 A/cm^2	≤ 0.01 A/cm^2
PIXEL UNIT CELL	Threshold voltage of VocP MOSFET	≥ 300 mV	≥ 400 mV	≥ 400 mV
PIXEL UNIT CELL	Noise	≤ 100 fA/√Hz	≤ 10 fA/√Hz	≤ 1 fA/√Hz
VOCP PIXEL	Dynamic range	≥ 3 o.o.m.	≥ 4 o.o.m.	≥ 5 o.o.m.
VOCP PIXEL	NEP at λ_{Peak}	≤ 500 pW/√Hz	≤ 100 pW/√Hz	≤ 10 pW/√Hz

4. PROJECT RESULTS

4.1 Fabrication of VocP Photovoltaic Detector

We fabricated isolated and series photovoltaic detectors from several heterostructure materials to assess their performance as V_{OC} generators and compatibility with the performance targets in Table 1. These materials are summarized in Table 2. Two of the materials were custom grown by OSU. The interband cascade photodetector (ICP) material was previously reported on [2, 3], and a limited set of diodes from that research were available for us in this project. Custom material grown by IntelliEpi was provided through the Air Force Research Laboratory (AFRL). Two commercially available photodetectors, Hamamatsu P13243 [4] and Asahi Kasei IR1011 [5], were acquired for testing because they have already been demonstrated to operate at 300 K. Both of these photodetectors use InSb as the absorber, grow the InSb on a semi-insulating GaAs substrate, and fabricate the detectors as a series of several photodiodes. Researchers at Asahi Kasei have published investigations into these photodetectors [6, 7] describing how the series of photodetectors leads to an improvement in the detector's SNR and enables room temperature operation with low responsivity but low dark current. We carried out several trials to fabricate custom series of high-responsivity materials, but none of these trials succeeded.

Table 2. Candidate PD Materials and Characterization Observations

IN FINAL TESTING?	MATERIAL	SUBSTRATE(S)	OBSERVED V_{OC}	ISOLATED OR SERIES?
Yes	OSU ICP [2, 3]	GaSb	Up to 300 mV @ 120 K, 2.6 W cm^{-2} sr^{-1}	Isolated
Yes	InAsSb Hamamatsu P13243 [4]	GaAs	100 mV @ 300 K, 2.6 W cm^{-2} sr^{-1}	Series
No	IntelliEpi IntelliEpi-M181207-045	GaSb	Up to 220 mV @ 80 K, 23 W cm^{-2} sr^{-1}	Isolated
No	IntelliEpi IntelliEpi-103185S 092 OPTO-370-MW-MnBn-02	GaAs	Not tested No successful fab	n/a
No	InSb Asahi Kasei IR1011 [5]	GaAs	92 mV @ 300 K , 2.6 W cm^{-2} sr^{-1}	Series
No	OSU InAsSb MOCVD	GaAs	Not tested No successful fab	n/a

The IntelliEpi-M181207-045 material was used to experimentally verify the expectation that the V_{OC} generated is independent of diode size. As shown in Figure 3, V_{OC} has a systematic dependence on diode temperature but no dependence on diode size in the range of 50 to 250 μm diameters.
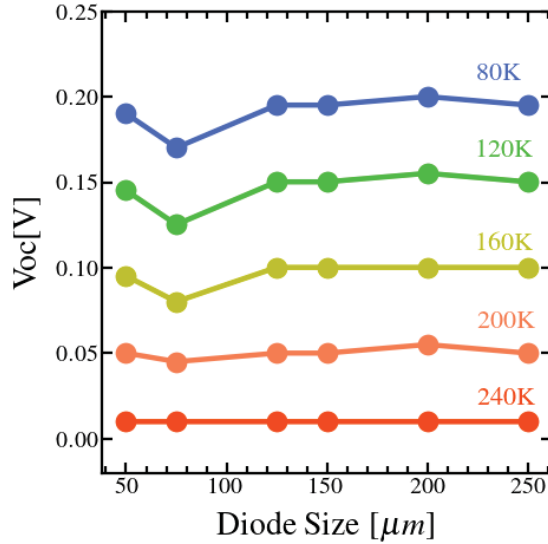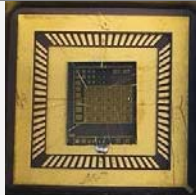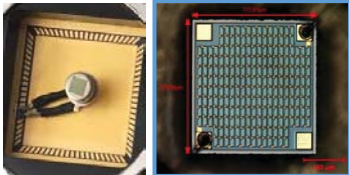
Figure 3: VOC generated from IntelliEpi-M181207-045 Diodes at a Constant Irradiance and Variations as a Function of the Diode operating Temperature and Size

Based on these fabrication and characterization, we selected two materials for integration and final testing. These are described and illustrated in Table 3. The H300 material enabled testing at room temperature, and the I77 material enabled testing of a single photodiode. The I77 material could be fabricated to provide a smaller pitch, but tests at these pixel sizes were not conducted. The H300 material, with diodes in a planar array, would be difficult to fabricate at a pitch as small as the target of 12 µm because the array is 15 diodes across. Despite this limitation, we chose to test H300 to have for a HOT detector. These Asahi Kasei and Hamamatsu detectors are state-of-the-art HOT detectors that have demonstrated performance at 300 K.

Table 3. Final Candidate PD Materials Integrated and Tested

CASE	MATERIAL	OPERATING TEMPERATURE	DETECTOR SIZE	INTEGRATION PHOTOGRAPH
I77	OSU ICP	77 K	400 µm	
H300	InAsSb Hamamatsu P13243	300 K	Series of 224 diodes, each ~40 µm	

4.2 Fabrication of VocP Custom ROIC

The VocP approach is predicted to generate signal photocurrents from fA to nA at relevant irradiance, with noise densities on the order of 1 fA/√Hz. Both of these are low enough that traditional analog measurement approaches will be challenged to accurately measure them. However, these are fully in-line with the capabilities of custom integrated circuits that integrate this current and measure a corresponding voltage change. Therefore, we designed, fabricated, characterized, and integrated a custom VocP ROIC with pixel unit cells.

The custom ROIC was designed and characterized by OSU, and it was fabricated by TowerJazz. OSU used the TowerJazz 180 nm CA18HD components as well as device models provided by TowerJazz in the design. OSU's ROIC (Figure 4) included 44 discrete VocP FETs, to enable testing of the integration of photovoltaic components with custom-designed FETs, and 24 distinct pixel unit cells. The pixel unit cells were arrayed (Figure 5) so that the devices reproduced any effects of neighboring pixels. Two pixel pitches were included, 10 μm and 20 μm.
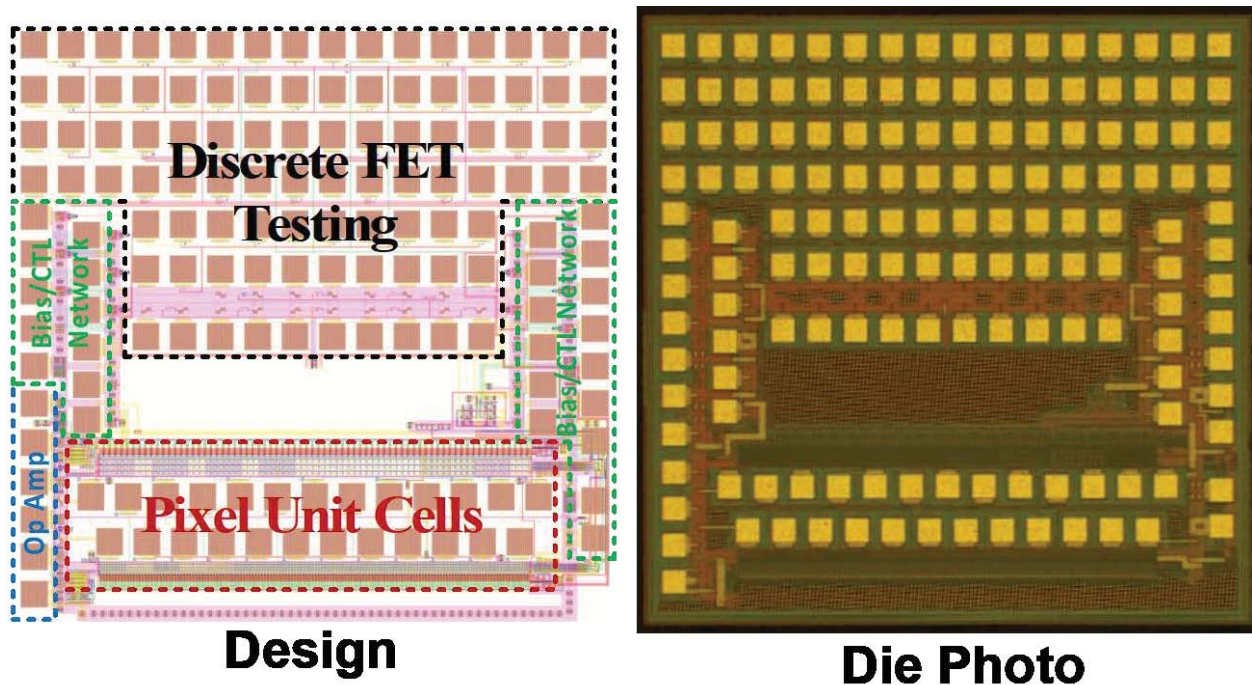
Figure 4: Schematic Illustration and Photograph of the Fabricated Die for the VocP ROIC
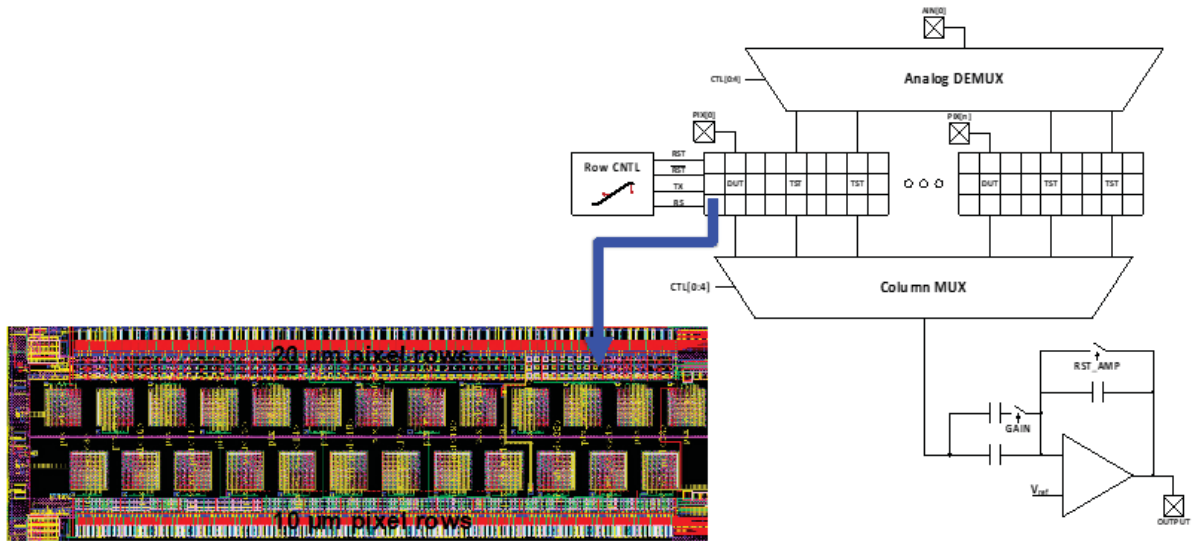
Figure 5: Illustrations of the Readout Architecture for the VocP ROIC

Because the VocP readout differs from complementary metal oxide semiconductor (CMOS) Image Sensor (CIS) and conventional PD ROIC operation, we designed and tested several variations in the pixel unit cells. In Figure 6, the key distinctions are:

a) 4T NMOS RST
b) 4T PMOS RST
c) 5T NMOS RST
d) 5T PMOS RST
e) 5T direct injection PMOS RST for testing PD configuration
f) Size variants of 4T/5T PMOS RST

Within these six designs, there were further variations tested in the oxide thickness and C_{INT}. These pixel flavors are listed in Table 4 and Table 5.
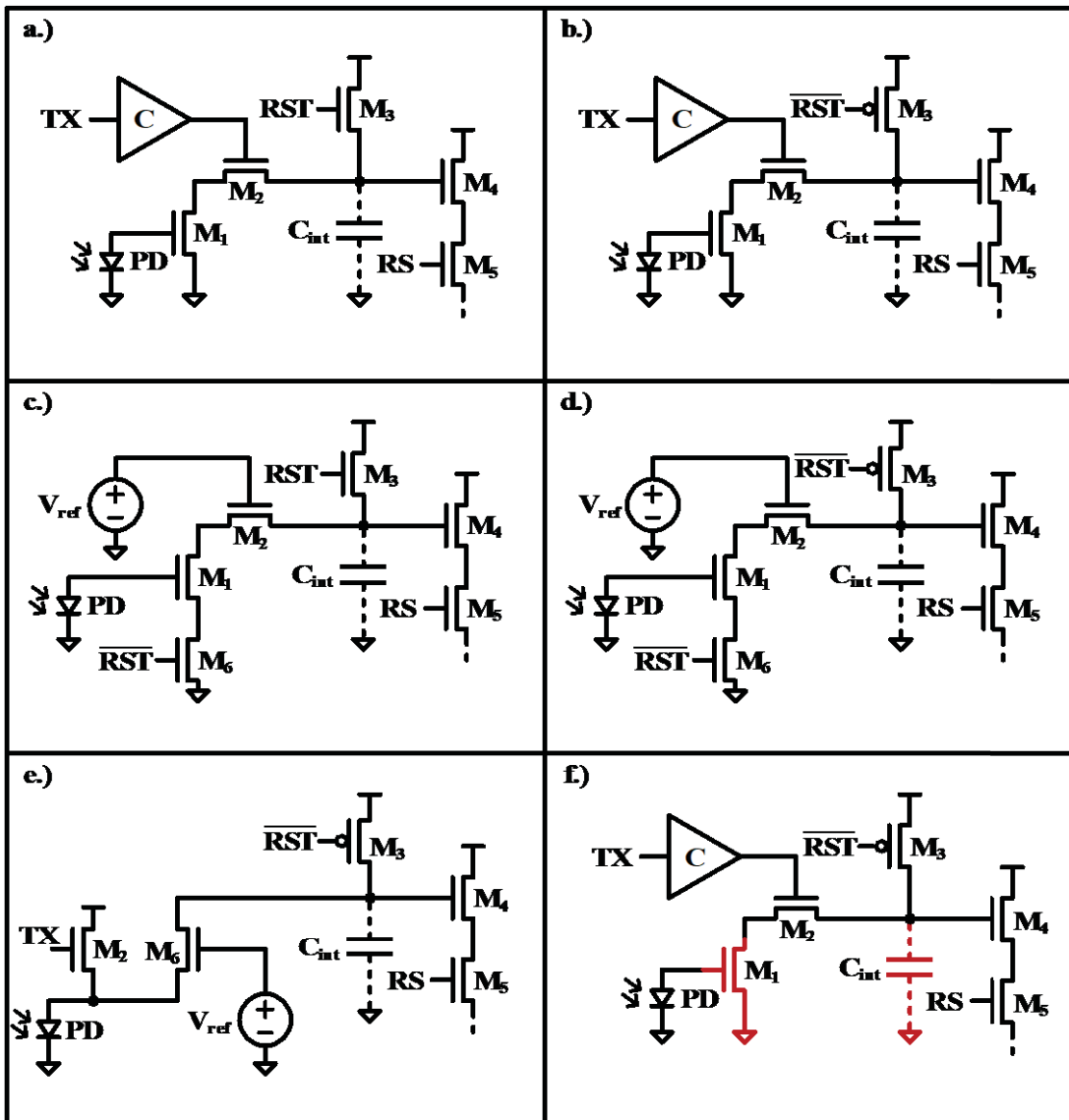
Figure 6: Pixel Unit Cells Designed, Modeled, and Fabricated

Table 4. Pixel Flavors, 20 μm Pitch

NUMBER	PIXEL TYPE	OXIDE	TRIPLE WELL?
1	b	Thin	Y
2	d	Thin	Y
3	a	Thin	Y
4	c	Thin	Y
5	b	Thick	N
6	d	Thick	N
7	e	Thick	N
8	f	Thin	Y

Approved for public release; distribution is unlimited.

Table 5. Pixel Flavors, 10 μm Pitch

NUM.	PIXEL TYPE	CINT	NUM.	PIXEL TYPE	CINT
9	d	50 fF	17	f	50 fF
10	b	25 fF	18	e	50 fF
11	e	50 fF	19	a(Cryo)	50 fF
12	d	25 fF	20	b(Cryo)	50 fF
13	e	25 fF	21	c(Cryo)	50 fF
14	a	50 fF	22	d(Cryo)	50 fF
15	b	50 fF	23	E	50 fF
16	c	25 fF	24	F	50 fF

Both modeling and testing of the fabricated pixel unit cells found that pixel # 1 (Table 4) provided the best performance as assessed by its inherent readout noise and compatibility with the fabricated photovoltaic detectors.

4.3 Test and Measurement

Measurements to quantify and compare the VocP detector performance were performed in four configurations as outlined in Figure 7. The Discrete measurements used a photovoltaic detector and one of the custom, discrete FETs on the custom ROIC. These components were wire bonded together and then connected to an analog current measurement system described further below. The discrete measurements eliminate the other circuit components and any noise or measurement complexity they introduce. The ROIC measurements use a pixel unit cell of the custom VocP ROIC. These unit cells required integration hardware and software described below. In both the Discrete and ROIC measurement configurations, comparative measurements were made of the signal and noise in PD and VocP mode.
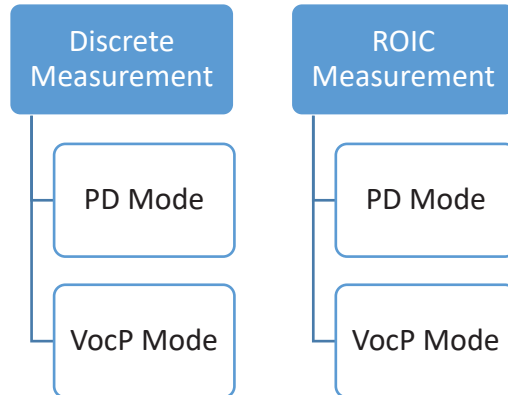

Figure 7: Overview of the Types of Measurements performed

4.3.1   Discrete Measurement Setup

The Discrete measurement setup is illustrated in Figure 8. The M1 FET was removed (PD mode) or inserted (VocP mode). The light source was chopped to generate an alternating current (AC) signal separated from a direct current (DC) background. The photocurrent, from the detector (I_{ph}) in the PD mode or from the FET (I_{ds}) in the VocP mode, was amplified using a low-noise trans-impedance amplifier (TIA) before being analyzed with a Fast Fourier Transform (FFT) spectrum analyzer. The signal and the noise were collected under different, calibrated radiation levels. The

light source was a calibrated blackbody radiator, and the radiation levels were controlled by changing its temperature, the size of an optical aperture, and the distance between the source and the detector. The data analysis separated the noise contributions of the amplifier and the FFT spectrum analyzer and accounted for the bandwidth of the test instruments. Figure 9 shows the Discrete measurement setup in use. The photodiodes were held in a cryostat for both the room temperature and low temperature measurements.
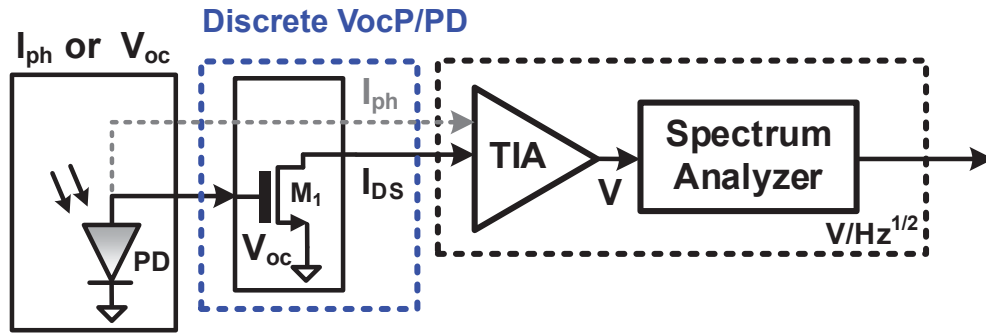

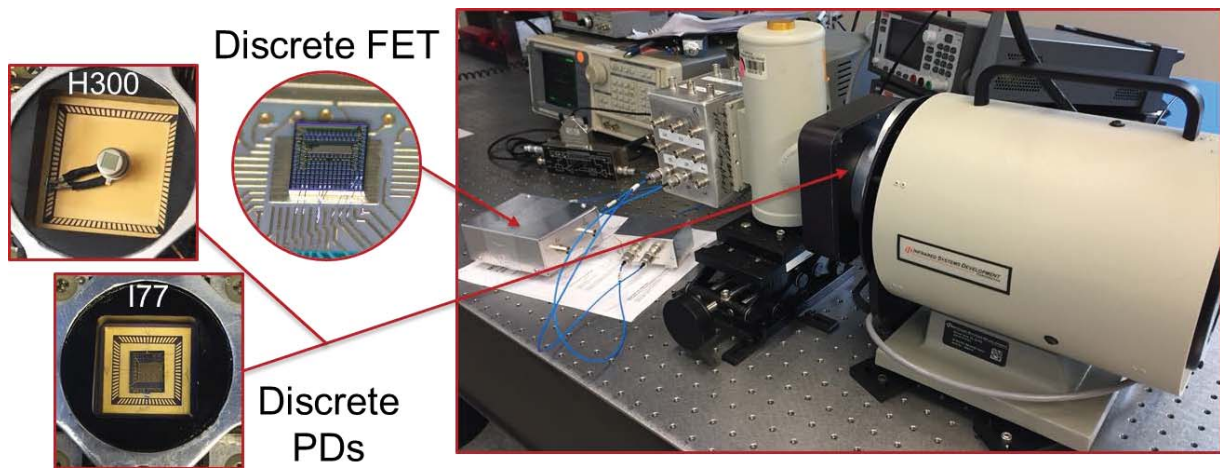**Figure 8: Schematic of the Discrete PD and VocP Measurement Setup**

Figure 9: Discrete VocP and PD Radiometric Measurements

The results of the Discrete measurements proved to be valuable for verifying the detector and FET performance characteristics at relatively high signal levels. However, as illustrated in Figure 10, the Discrete measurements accuracy were limited by the measurement system at low signal levels. The TIA, at the needed bandwidth, has a noise floor limit of 11.5 fA/√Hz. The measurements of the VocP mode had a noise level below this. Therefore, the Discrete measurements provided confirmation and extension of the ROIC measurements but were not able assess the VocP performance at the limit of detection.
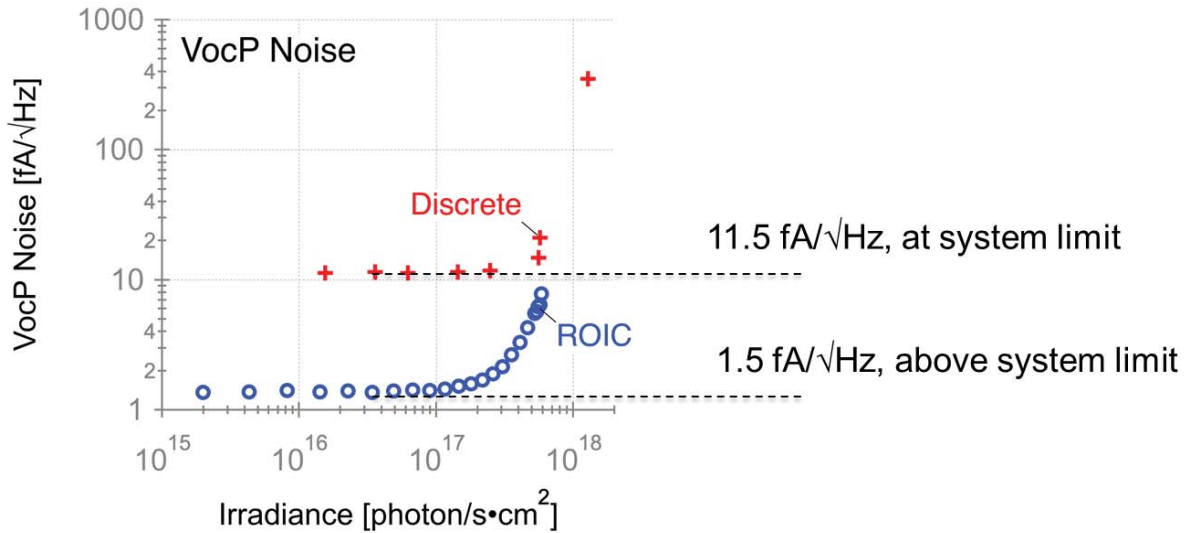
Figure 10: Measured Noise Spectral Density for H300 VocP
The Discrete and ROIC setups are compared.

4.3.2   ROIC Measurement Setup

Figure 11 illustrates the signal path of the VocP and PD modes in the ROIC test measurements. Details of the custom unit pixel cell were provided in previous reports. The intention of the test readout design shown in Figure 11 was to limit the noise addition from the components in the chain that succeed the pixel unit cell. In this way, the noise of each unit cell, as well as the root mean square (RMS) sum of the noise from the PD and pixel unit cell, can be isolated and measured accurately. For this reason, a 16-bit precision analog to digital converter (ADC) is used to ensure that the quantization noise floor falls well below the noise floor created by the input devices. Testing determined that the unit pixel cell had a noise contribution <1 fA/√Hz, and this enabled the VocP noise measurement down to 1.5 fA/√Hz illustrated in Figure 10.
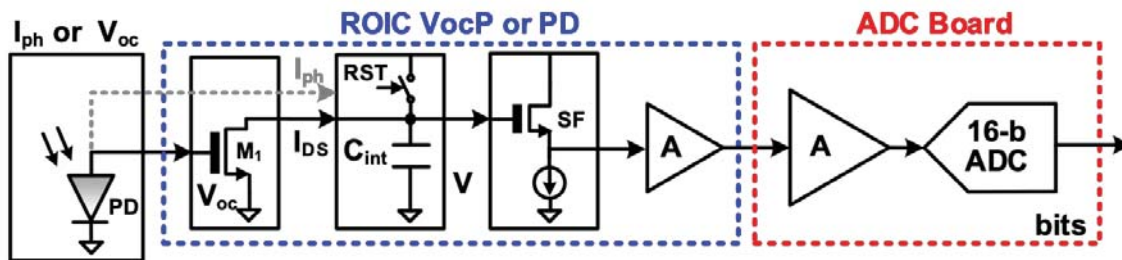
Figure 11: ROIC Characterization Platform Signal Path & Noise

Figure 12 shows the test setup for the PD and readout characterization using the VocP ROIC and characterization platform. The PD is placed in a cryostat with a 3.5-5 μm bandpass filter to isolate the region of peak responsivity of the PD corresponding to the MWIR spectrum. A calibrated blackbody irradiates the PD, and the blackbody temperature is varied to vary the MWIR irradiance.
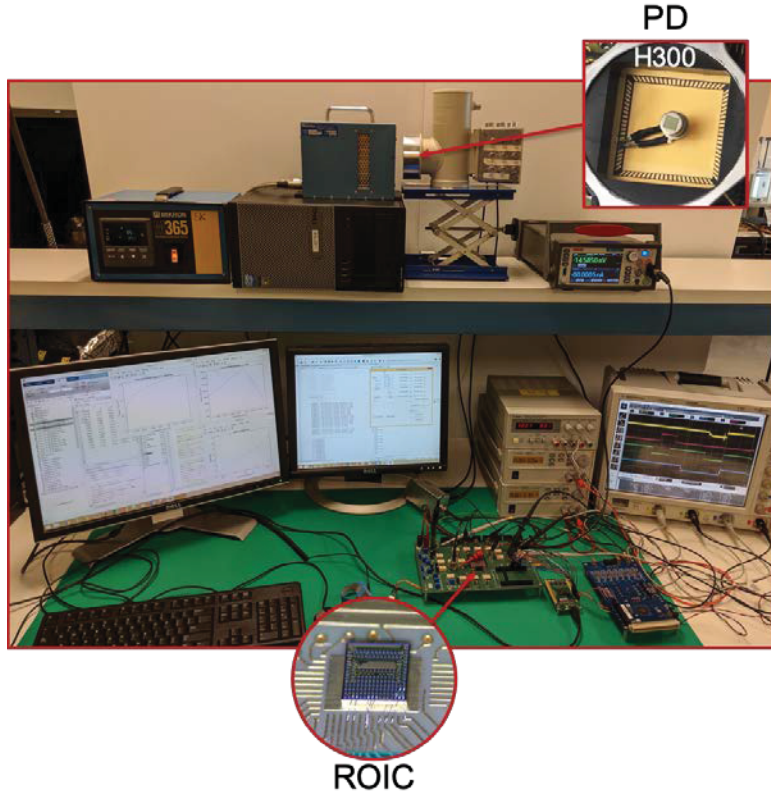
Figure 12: ROIC VocP and PD Radiometric Measurements

The PD is connected to the ROIC development platform, a custom interface board, though BNC connectors. When testing the VocP mode, the PD is forward biased and connected directly to the gate of the NMOS FET device (M1) in the VocP pixel. Similarly, the commercial photodiode used in the VocP mode is evaluated under the same readout and pixel unit cell conditions. The only difference between the VocP and conventional PD setups, as illustrated in Figure 11, is the absence of the M1 transistor in the PD setup, making the pixel unit cell identical to the well-known direct injection topology. The differences between the two test cases, as well as the signal path of both VocP and photocurrent readout modes, is shown in Figure 11. It is important to note that the C_{INT} is the same in the two modes because a single pixel unit cell is under test. As expected, the PD mode has a signal current that is several orders of magnitude higher. To compensate for this, and not fill the capacitor, the PD integration time is less than the VocP integration time. This leads to a difference in output bandwidth that has to be accounted for in the comparisons.

4.4 Model of VocP Detector and ROIC

The measured signal vs. irradiance was compared to analytical models of the PD (Eq. 1) and sub-threshold FET (Eq. 2) response. In Eq. 1 V_{OC} is the open-circuit voltage, N is the number of photodiodes in series, n_{Diode} is the diode ideality coefficient, T_{Diode} is the diode operating temperature, E_λ is the irradiance, R_λ is the diode responsivity, and J_{sat} is the diode saturation current density. In Eq. 2 I_{DS} is the drain-source current, $I_{S,s-t}$ is the FET threshold drain current, V_{Th} is the FET threshold voltage, n_{FET} is the FET ideality coefficient, and V_{GS} is the gate-source

voltage. In the VocP mode, V_{GS} is equal to V_{OC}, and the combination of the two equations leads to Eq. 3. As illustrated in Figure 13, these models accurately fit the measured data at various irradiance levels. Figure 13 illustrates the measured data and least squares fits for the ROIC measurements of H300 in the VocP mode. The best-fit characteristics of the PD are consistent with the manufacturer's specifications and of the FET are consistent with the TowerJazz design specifications.

$$V_{OC} = N\, n_{Diode}\, \frac{k_B T_{Diode}}{q}\, \ln\left(1 + E_\lambda\, \frac{R_\lambda}{J_{Sat}}\right) \qquad \text{Eq. 1}$$

$$I_{DS} = I_{S,s-t}\, \exp\left(-\frac{V_{Th}}{n_{FET}}\frac{q}{k_B T_{FET}}\right) \exp\left(\frac{V_{GS}}{n_{FET}}\frac{q}{k_B T_{FET}}\right) \qquad \text{Eq. 2}$$

$$I_{Signal} = I_{Leak}\left[\left(E_\lambda\, \frac{R_\lambda}{J_{Sat}} + 1\right)^\beta - \left(E_{\lambda,Bkg}\, \frac{R_\lambda}{J_{Sat}} + 1\right)^\beta\right] \qquad \text{Eq. 3a}$$

$$\beta = \frac{N\, n_{Diode} T_{Diode}}{n_{FET} T_{FET}} \qquad \text{Eq. 3b}$$

$$I_{Leak} = I_{S,s-t}\, \exp\left(-\frac{V_{Th}}{n_{FET}}\frac{q}{k_B T_{FET}}\right) \qquad \text{Eq. 3c}$$
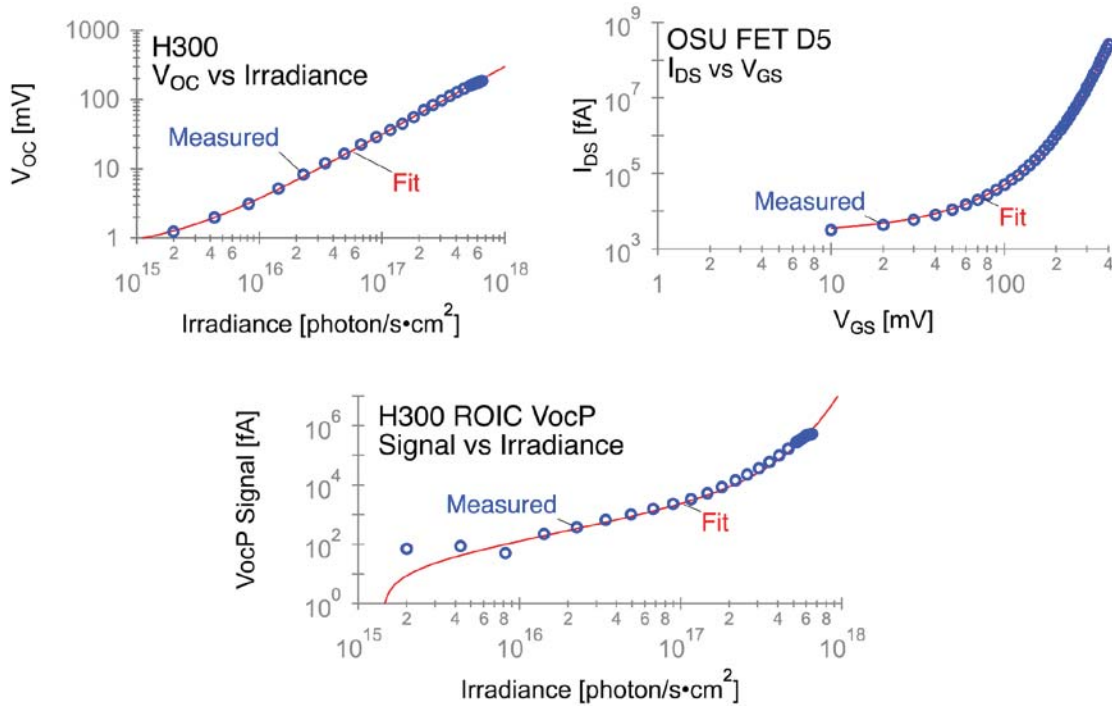

Figure 13: ROIC VocP Signal compared to Least Squares Fits to the Analytical Signal Models

In addition to this analytical signal model, we developed a circuit noise model. The noise model, illustrated in Figure 14, accounts for the circuit readout noise, the FET thermal noise (flicker noise was considered but found to be negligible), and the PD noise. In the PD mode, the sources of noise are well established to be the diode's thermal/Johnson noise (Eq. 4) determined by its shunt resistance (R_{Sh}) and its shot noise (Eq. 5) determined by both the photo and dark current. In the VocP mode, all sources of noise relate to the FET's g_m factor (Eq. 6) which is itself dependent on V_{GS}. The two dominant contributors to the VocP mode noise are the FET Johnson noise (Eq. 7) and the photovoltaic source's equivalent resistor noise (Eq. 8a) translated into the FET current noise (Eq. 8b). This model is not analytical because the g_m factor of the FET is dependent on the V_{GS} level.
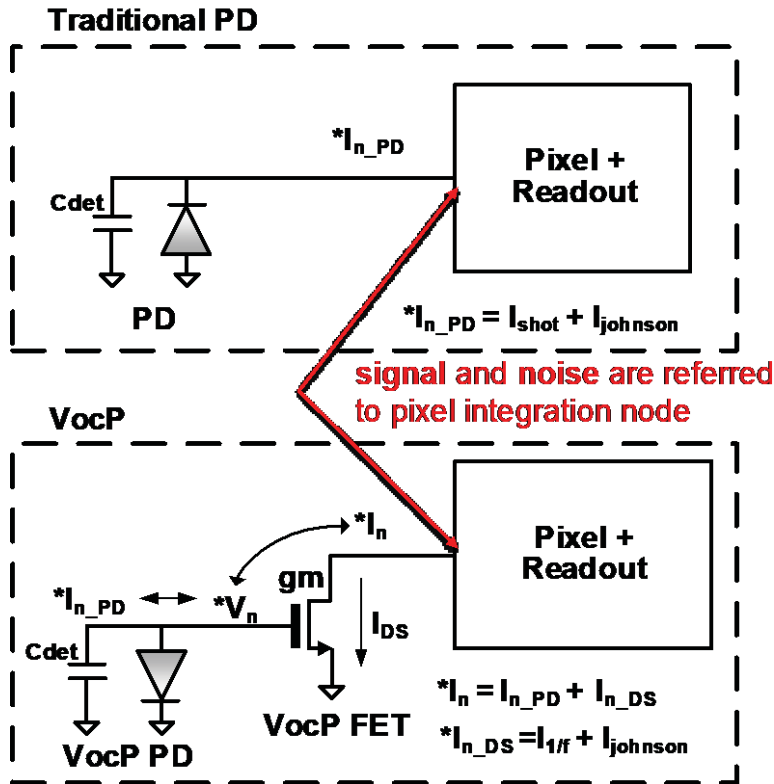

Figure 14: Circuit Schematics for the Noise Model of the PD (top) and VocP (bottom) Modes

$$I_{n,thermal}^2 = \frac{4k_B T}{R_{sh}} \Delta f$$

<div align="right">Eq. 4</div>

$$I_{n,shot}^2 = 2q(I_{Ph} + I_{Dark})\Delta f$$

<div align="right">Eq. 5</div>

$$g_m = \frac{d(I_{DS})}{d(V_{OC})} = \frac{I_{DS}}{nV_t}$$

<div align="right">Eq. 6</div>

$$I_{n,Johnson}^2 = 2k_B T n g_m \Delta f$$

<div align="right">Eq. 7</div>

$$V_{n,OC}^2 = 4k_B T R_{sh} \Delta f$$

<div align="right">Eq. 8a</div>

$$I_{n,OC}^2 = g_m^2 V_{n,OC}^2 = g_m^2 4k_B T R_{sh} \Delta f$$

<div align="right">Eq. 8b</div>

Figure 15 compares the ROIC measured noise characteristics to model results in the low irradiance range. The model predictions use the manufacturer's specifications, for the PD, and design specifications, for the FET. Close agreement between measurement and model are achieved in this plot for both the VocP mode, as well as the traditional PD mode. The measured noise is input-referred in both cases. The VocP noise is orders of magnitude lower than the PD noise. This is expected because the VocP noise limit is dictated by the leakage current of the FET, ~1 pA for the 180 nm technology used for this ROIC. The PD noise limit is dictated by the shot noise due to the diode dark current, several nA for the H300.
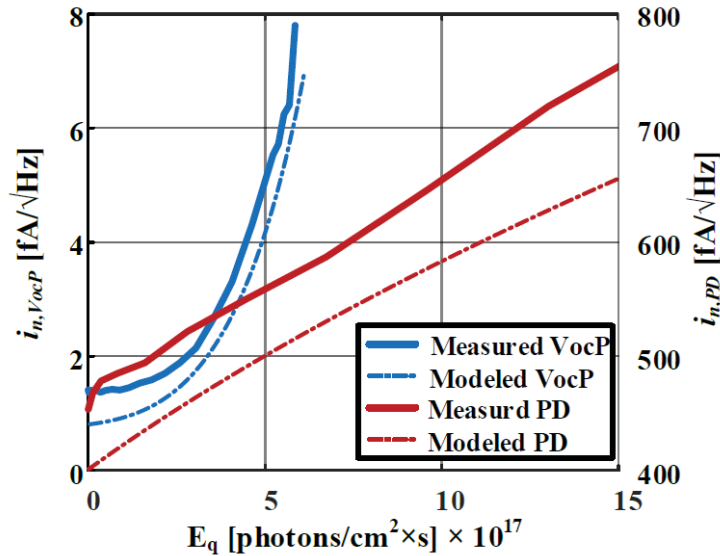

Figure 15: Measured and Modeled Input-referred Current Spot Noise vs. Photon Irradiance for both the Conventional PD (right axis) and the VocP (left axis) Pixels using the H300 Photodetector at Room Temperature

4.5 Analysis & Conclusions

The measured and modeled SNR for the H300 are shown in Figure 16. First, the close match between measured and modeled results supports the model we developed. Second, a sensitivity improvement is seen using the VocP topology over the conventional, PD counterpart. An analysis of the NEP, that accounts for the differing noise bandwidths, finds that the conventional PD's NEP is 1.53 nW/√Hz (integration time of 50 ns), four times lower than the VocP's NEP of 6nW/√Hz (integration time of 42 μs). These results confirm that the VocP mode is competitive, and the confirmation of the model enable us to design the VocP to improve its performance further.
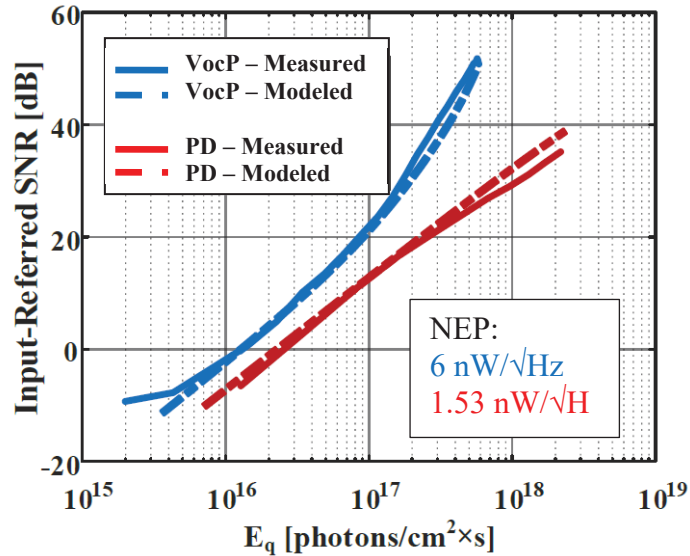
Figure 16: Measured and Modeled SNR vs. Photon Irradiance for both the Conventional PD and the VocP Pixels using the H300 Photodetector at Room Temperature

Table 6 compares the measured characteristics of the H300 and I77 demonstration cases against the project performance targets. The Pixel Unit Cell design met the targets for both a Phase I and II, and the lessons learned point to a path to surpass Phase III. The photovoltaic comparison cases had significantly lower dark currents than the targets, surpassing this specification, but failed to meet the responsivity specification. One of the lessons learned from the improved VocP model is that the responsivity and dark current are not significant independently; instead, their ratio is a factor in determining the V_{OC} sensitivity of the photovoltaic (Eq. 1). Future specifications for a VocP material will place the emphasis on this V_{OC} generation instead of responsivity and dark current. The pixel dynamic range met our Phase I target, and there is a clear design path to increase that by adjusting the integration capacitor and decreasing the NEP. The demonstrated NEP did not meet the target, and this is discussed further below in the context of design forecasts.

Table 6. Performance Assessment of Components and Integrated VocP Detector against the Phase I Targets

Targets shaded in green were met or exceeded. Targets shaded in yellow were met in one demonstration but not the other, and targets shaded in red were missed.

COMPONENT	CHARACTERISTIC	H300	I77	PHASE I
PHOTOVOLTAIC	Pitch	375 µm Tested	400 µm Tested	Compatible with 12 µm
PHOTOVOLTAIC	Operating Temperature	300 K	77 K	At 300 K
PHOTOVOLTAIC	Peak response wavelength (λ_{Peak})	4 µm	4 µm	Between 3-5 µm
PHOTOVOLTAIC	Responsivity at λ_{Peak}	8.7 mA/W	97 µA/W	$\geq$ 0.1 A/W
PHOTOVOLTAIC	Dark current density at −5 mV	1.0 mA/cm^2	1.5 µA/cm^2	$\leq$ 1 A/cm^2
PIXEL UNIT CELL	Threshold voltage of VocP MOSFET	400 mV	400 mV	$\geq$ 300 mV
PIXEL UNIT CELL	Noise	1.5 fA/√Hz	1.5 fA/√Hz	$\leq$ 100 fA/√Hz
VOCP PIXEL	Dynamic range	3 o.o.m.	3 o.o.m.	$\geq$ 3 o.o.m.
VOCP PIXEL	NEP at λ_{Peak}	6 nW/√Hz	2 nW/√Hz	$\leq$ 500 pW/√Hz

We used the improved, and experimentally verified, detector model to re-assess and compare the projected performance of an optimal VocP detector. Figure 17 compares the SNR predictions for a state-of-the-art photodiode in VocP and PD modes. The predicted NEP for the VocP mode is superior to the PD mode and comparable to the MWIR HgCdTe detectors in use today. The model we have developed will now allow us to explore the design space of available diodes and FETs to achieve a performance target.

Modeled Characteristics

- Pixel: $QE = 0.5$, 10 μm pitch
- *Diode:* $R_{sh} = 35$ MΩ, $I_{Sat} = 1$ pA, $n_D = 1$
- *FET:* $V_{th} = 0.34$ V, $n_{FET} = 1.23$, $I_{leakage} = 1$ pA
- $T_{int} = 20$ μs, $\Delta f = 25$ kHz (VocP)
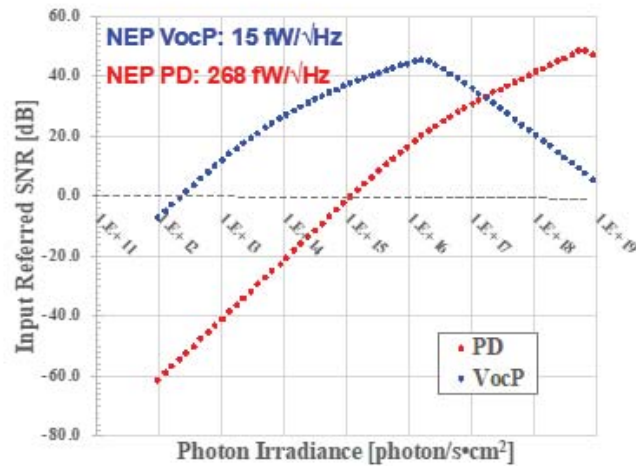- $T_{int} = 50$ ns, $\Delta f = 20$ MHz (PD)

Figure 17: Comparison of Modeled VocP and PD Sensitivity for a State-of-the-Art PD and FET

One valuable aspect of VocP that our work uncovered is that there are cases where the PD contribution to the VocP noise limit is insignificant. In these cases, the FET thermal noise alone determines the low-signal noise limit. The model predicts this result for photodiodes with sufficient shunt resistance. This relaxes the normally stringent requirements for shunt resistance in most state-of-the-art MWIR detectors, and it allows for this performance burden to be passed on to the M1 transistor operating in the subthreshold region. The performance of this transistor is extremely well controlled compared to the exotic materials used to fabricate MWIR PDs, and this performance gap is even greater when operating at room temperature.

Our work with the VocP detector and ROIC has led to the identification of two performance benefits that we had not previously recognized. First, the fact that the VocP ROIC does not apply a bias voltage to the diode will reduce the ROIC power consumption. Further quantitative modeling and testing will be needed to determine the overall power benefits of this change. Second, the reduction in the photocurrent signal, by several orders of magnitude without sacrificing sensitivity, provides a path to improved high-speed IR imaging. The proposed VocP architecture shows that imaging at kfps and above can be achieved using the minimum sized metal-insulator-metal (MIM) capacitor that the technology has to offer for the per-pixel integration capacitor. Therefore, VocP promises better sensitivity at high frame rates.

5. PATH FORWARD AND OUTLOOK FOR VOCP DEVICES

We demonstrated the feasibility of implementing a VocP detector by operating a photodetector in an open-circuit voltage configuration and using it to control the gate-source voltage of a FET. We developed two experimental platforms for characterizing this approach and also made comparison measurements to a more traditional PD configuration. We developed a model of the detector system that accurately predicts the signal and noise performance of a VocP detector and enables further design work.

Our experimental and theoretical assessments identified the following advantages for a VocP detector:

- Pixel size reduction without a signal penalty (experimentally verified) and with a smaller noise penalty (predicted) than a traditional photocurrent approach
- Predicted NEP improvement by operation in VocP configuration over a traditional photocurrent configuration
- A reduction in the size of the ROIC integration capacitors, by several orders of magnitude, due to the reduction in the baseline, dark photocurrent. This supports reducing the pixel pitch and takes advantage of visible imager sensor technologies
- The possibility of sensitive, high-speed imaging with these smaller capacitors
- A reduction in ROIC power demands by not applying a bias voltage to the photodiodes
- A resilience to the increase of photodiode dark current as operating temperature increases. The ROIC design does not need to change, since the integration capacitors are sized to match the FET, and a detector approach such as H300 can maintain sufficient V_{OC} sensitivity.

The near- and long-term next steps to continue to develop and improve the VocP include:

- Near-term study of the open circuit voltage noise and its propagation into the VocP pixel unit cell
- Near-term improvements in the fabrication of smaller diodes, in the range of 6 to 50 μm, to support assessments of V_{OC} signal and noise in this size range
- Near-term improvements in the usability of the ROIC measurement system to support further, systematic electro-optical characterization of combinations of detectors and pixel unit cells
- Near-term performance assessments, experimental and theoretical, using noise equivalent temperature (NET) as the metric to directly account for optimization of integration times and integration capacitance for the VocP and PD modes
- Long-term assessment and optimization of photovoltaic materials to optimize system performance targets such as NET, read-out speed, pitch, and operating temperature
- Long-term assessment and optimization of VocP pixel unit cells to optimize system performance targets such as NET, read-out speed, pitch, and operating temperature
- Long-term assessment of FPA assembly strategies for VocP FPAs

6. PROJECT PUBLICATIONS AND PRESENTATIONS

As of January 2020, the public presentations resulting from this project are:

- Specht, T., Z. Taghipour, T. J. Ronningen, R. Fragasse, R. Tantawy, S. Smith, E. Fuller, W. Khalil and S. Krishna (2019). "Novel photodetector design using open circuit voltage for mid-wave infrared imagers." SPIE Defense + Commercial Sensing, SPIE.
- Teressa Specht, Z. Taghipour, R. Fink, R. G. Fragasse, R. Tantawy, T. J. Ronningen, S. Smith, E. Fuller, W. Khalil, S. Krishna (2019). "Open Circuit Voltage Photodetector (VocP) Architecture for Mid-wave Infrared Imagers." Ohio State University SSEP Seminar Series.
- Roman Fragasse, Ramy Tantawy, Shane Smith, Teressa Specht, Zahra Taghipour, Phillip Van Hooser, Christopher Taylor, Theodore J. Ronningen, Earl Fuller, Rudy Fink, Sanjay Krishna and Waleed Khalil (2020) "Advancing Uncooled Infrared Imagers Using An Open-Circuit Voltage Pixel." LASCAS 2020.

7. REFERENCES

[1]   R. C. Jones, "Phenomenological Description of the Response and Detecting Ability of Radiation Detectors," *Proceedings of the IRE,* vol. 47, no. 9, pp. 1495-1502, 1959, doi: 10.1109/JRPROC.1959.287047.

[2]   Z. B. Tian, S. E. Godoy, H. S. Kim, T. Schuler-Sandy, J. A. Montoya, and S. Krishna, "High operating temperature interband cascade focal plane arrays," *Applied Physics Letters,* vol. 105, no. 5, p. 051109, 2014, doi: 10.1063/1.4892634.

[3]   Z. B. Tian, S. E. Godoy, H. S. Kim, T. Schuler-Sandy, J. Montoya, and S. Krishna, "Mid-wave infrared interband cascade photodetectors and focal plane arrays," in *Infrared Technology and Applications Xl*, vol. 9070, B. F. Andresen, G. F. Fulop, C. M. Hanson, and P. R. Norton Eds., (Proceedings of SPIE. Bellingham: SPIE-Int Soc Optical Engineering, 2014.

[4]   Hamamatsu. *P13243 Series*, Hamamatsu, 2018. [Online]. Available: https://www.hamamatsu.com/us/en/product/type/P13243-011MA/index.html. Accessed: 2018-07-16.

[5]   A. Kasei. *IR1011 Photovoltaic Infrared Sensor*, Asahi Kasei, 2012.

[6]   K. Ueno *et al.*, "InSb Mid-Infrared Photon Detector for Room-Temperature Operation," *Japanese Journal of Applied Physics,* vol. 52, no. 9R, 2013, doi: 10.7567/jjap.52.092202.

[7]   E. G. Camargo *et al.*, "Performance Improvement of Molecular Beam Epitaxy Grown InSb Photodiodes for Room Temperature Operation," *Japanese Journal of Applied Physics,* vol. 47, no. 11, pp. 8430-8433, 2008/11/14 2008, doi: 10.1143/jjap.47.8430.

8. ADDENDUM

The attached presentation on "Photodiode Noise Models" was prepared by Josh Duran, Gamini Ariyawansa, and Charles Reyner of AFRL. These researchers performed the reported measurements and modeling as an independent assessment of some aspects of the reported VocP results.

Photodiode Noise Models

Reverse Bias vs V_{oc} Mode

AFRL
THE AIR FORCE RESEARCH LABORATORY
LEAD | DISCOVER | DEVELOP | DELIVER

Josh Duran
Gamini Ariyawansa
Charles Reyner

Goals

- Review and understand photodiode noise models (as a function of bias)
- Measure noise at V_{oc} and fit to models
- Use models to predict FPA performance under various conditions (comparing V_{oc} mode to reverse bias)
- Determine whether there is a path forward using today's detector technology

Photodiode Noise Models

Johnson Noise Model

- Shot noise considered only for biases with net current.
- Dark noise at zero bias is reduced to Johnson Noise.
- Illuminated noise is reduced Johnson Noise at V_{oc}.

$$i^2_{nois_e} = \left(\frac{4k_BT}{r_d} + 2qi\right)\Delta f$$
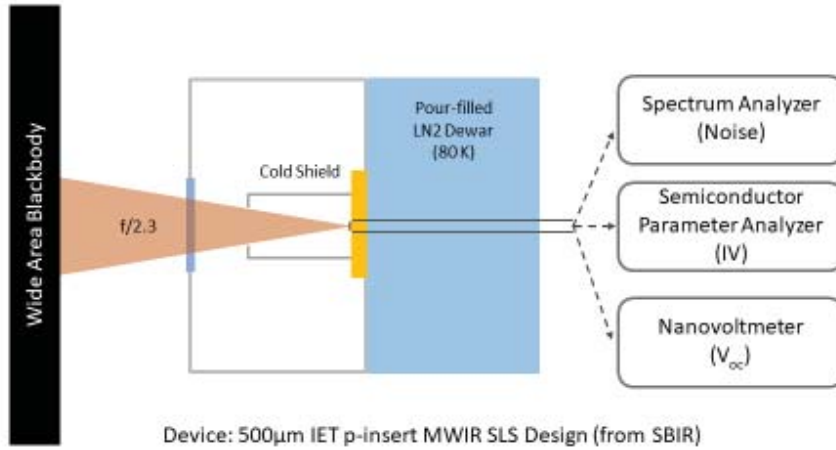
$$v^2_{nois_e} = \left(4k_BTr_d + 2qi_tr_d^2\right)\Delta f$$

Johnson & Shot Noise Model

- Shot noise considered even when net current is zero.
- Both positive and negative currents (which net to zero) contribute to shot noise.
- Same Johnson noise also present.
- Buckingham and Faulkner, The Radio and Electronic Engineer, Vol. 44, No. 3, 1974 (Derivation)

$$i^2_{nois_e} = \left(\frac{4k_BT}{r_d} + 2q|i_d + 2i_s| + 2qi_{ph}\right)\Delta f$$

$$v^2_{nois_e} = \left(4k_BTr_d + 2qr_d^2(|i_d + 2i_s| + i_{ph})\right)\Delta f$$

Test Setup

Pour-filled LN2 Dewar (80 K)

Cold Shield

Wide Area Blackbody

f/2.3

Spectrum Analyzer (Noise)

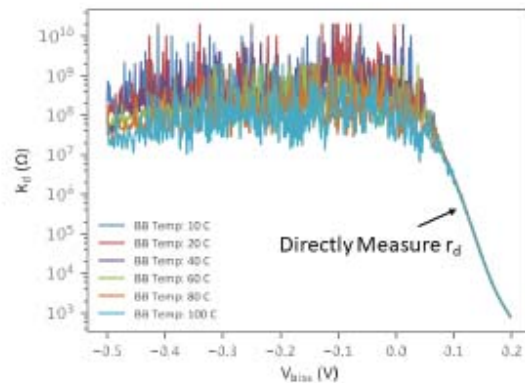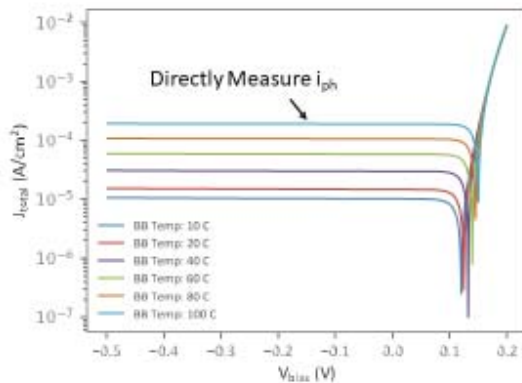Semiconductor Parameter Analyzer (IV)

Nanovoltmeter (V_{oc})

- Measuring noise spectrum (voltage) by directly connecting the device under illumination to the spectrum analyzer.
- Use IV curves from the SPA to get i_{ph} and r_d.
- Nanovoltmeter is used to more accurately measure V_{oc}. This is important because of the exponential dependence of r_d on V (SPA not precise enough)

Device: 500μm IET p-insert MWIR SLS Design (from SBIR)

Extracting Unknowns from Measurement

$$v_{noise(J)}^2 = \left(4k_B T r_d + 2q i_t r_d^2\right)\Delta f \qquad v_{noise(J\,\&}^2 = \left(4k_B T r_d + 2q r_d^2\left(|i_d + 2i_s| + i_{ph}\right)\right)\Delta f$$

Directly Measure i_{ph}

Directly Measure r_d

At V_{oc} only remaining unknown is i_s

Fitting the Shockley Eq. to Illuminated IV Data

$$i_t = i_s\left(e^{qv_b/nk_BT} - 1\right) - i_{ph} + \frac{v_b}{r_{sh}}$$

n: 1.55
i_s: 3.5e-13 A
r_{sh}: 5e8 Ω
i_{ph}: i_t @ 0V
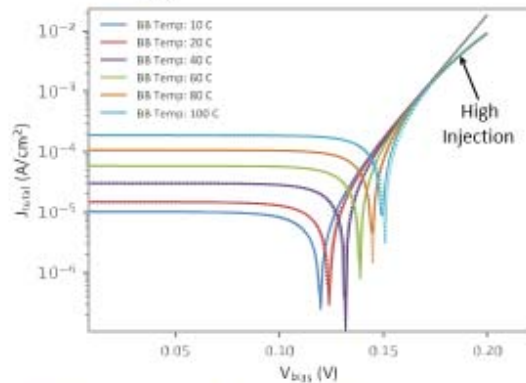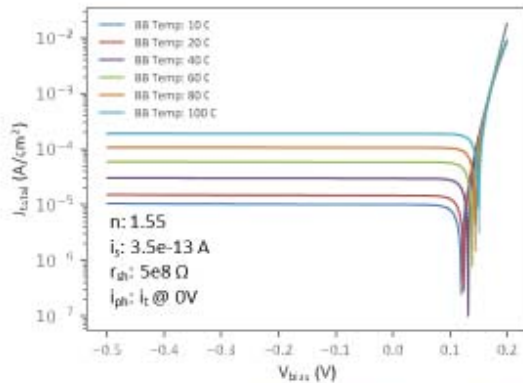
High Injection

i_s is negligible under these conditions so can be ignored
Shockley equation is not valid under high injection conditions
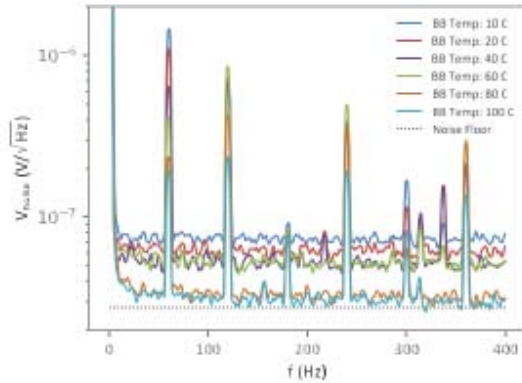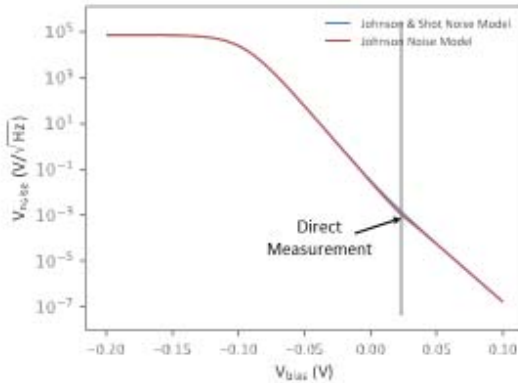
Noise Measurement Calibration (Resistors)
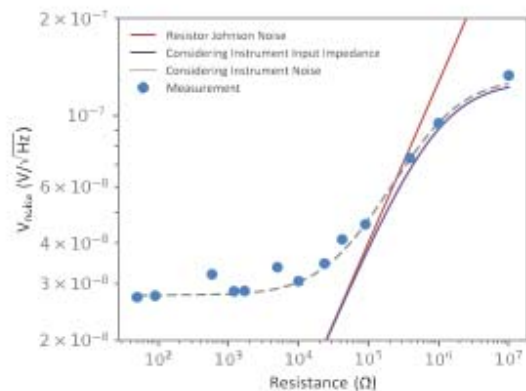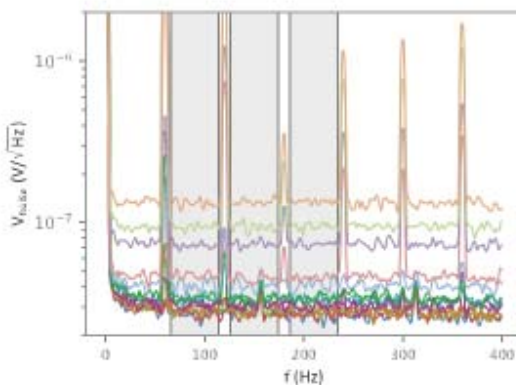
$$r_{ef} = \frac{r + r_{input}}{r + r_{input}} \qquad V_{J(reff)} = 4k_BTr_{ef} \qquad = \frac{V_{Jinput} + V_{Jdevice}}{V_{Jinp} + V_{Jdevi}} \qquad V_{noise} = \sqrt{V_{J(reff)}^2 + V_{floo}^2}$$
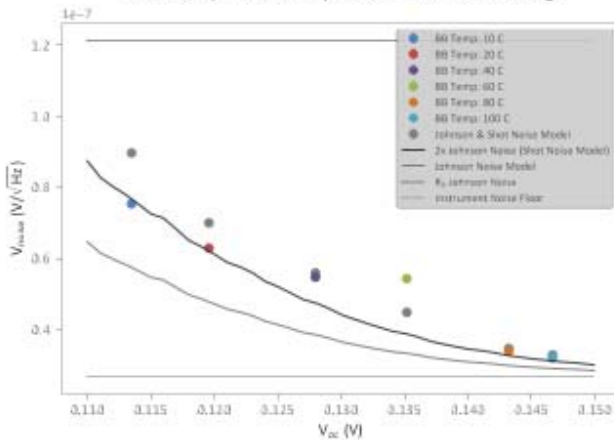
V_{OC} Noise Spectrum

1/f not significant

Voltage Noise Measurement
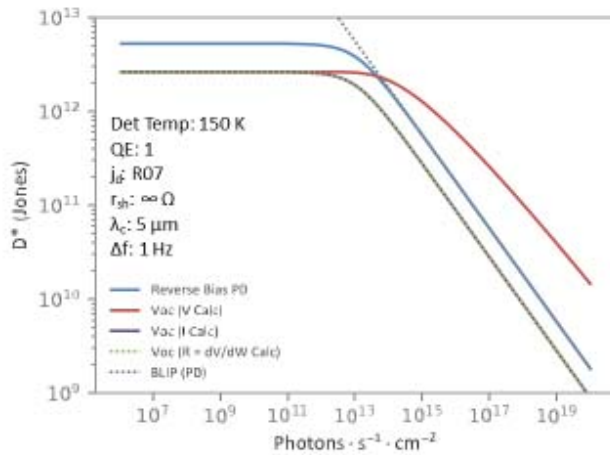
f/2.3 500µm 80K IET p-insert MWIR SLS Design

- Photon current taken to be absolute current at zero bias from IV curve.
- Shunt impedance taken directly from measurement.
- Dynamic impedance used for Johnson noise calculation.
- Input impedance and noise floor of the analyzer must be considered when modeling the noise (input impedance at room temp).
- V_{oc} Measured with nanovoltmeter
  - Small errors in V_{oc} are amplified by the exponential dynamic impedance.
- Noise measured by directly connecting illuminated device to spectrum analyzer
- Model that includes shot noise fits better to the measurement, but more data should be taken.

We can reasonably model the noise at Voc: use that to predict FPA performance
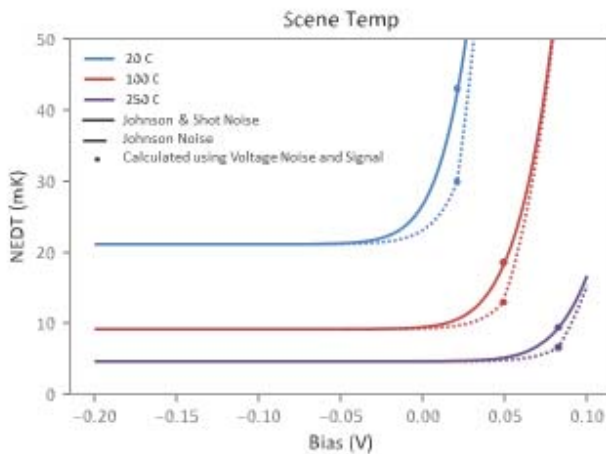
Performance Metrics: D*

$$D^* = \frac{R\sqrt{A}}{S_n}$$

Det Temp: 150 K
QE: 1
j_d: R07
r_{sh}: ∞ Ω
λ_c: 5 µm
Δf: 1 Hz

Legend:
- Reverse Bias PD
- Voc (V Calc)
- Voc (I Calc)
- Voc (I = dV/dW Calc)
- BLIP (PD)

Axis: D* (Jones) vs Photons · s⁻¹ · cm⁻²

- D* calculation using voltage responsivity and noise does not agree with D* calculation using current responsivity and noise (in V_{oc} mode).
- Due to nonlinear voltage responsivity.
  - We believe linear responsivity is implied by the D* definition (or responsivity is defined as a differential).
  - Must use differential responsivity to calculate D* (or meaningful SNR)
- This can explain OSU's higher SNR measurement for VocP vs standard photodiode and suggests this is not a good metric to use, as it can be misleading.

Performance Metrics: NEDT

Scene Temp

Legend:
- 20 C
- 100 C
- 250 C
- Johnson & Shot Noise
- Johnson Noise
- • Calculated using Voltage Noise and Signal
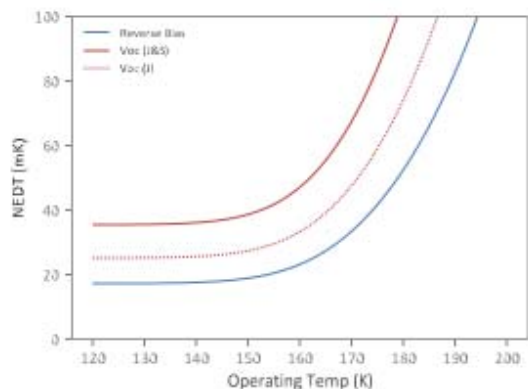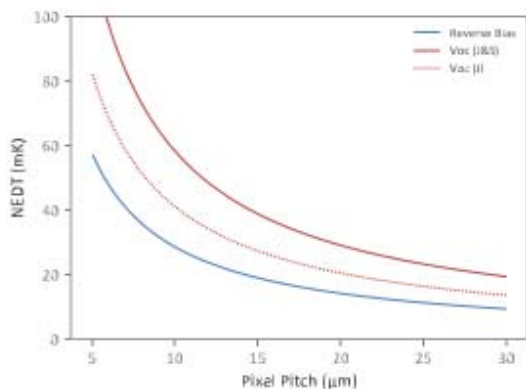
Axis: NEDT (mK) vs Bias (V)

$$NEDT = \Delta T \frac{Noise_{lo}}{Sig_{high} - Sig_{low}}$$

- NEDT Calculation agrees whether we use voltage signal and noise (dots) or current signal and noise (lines).
- NEDT is a more straightforward metric because it doesn't require linear responsivity.
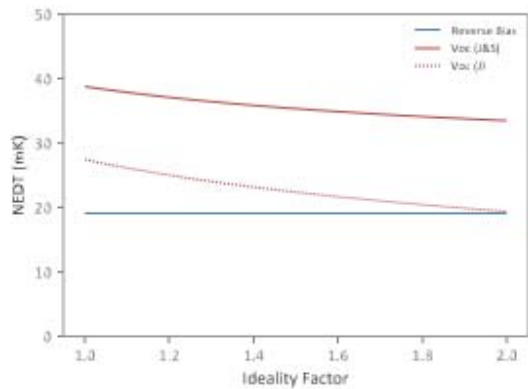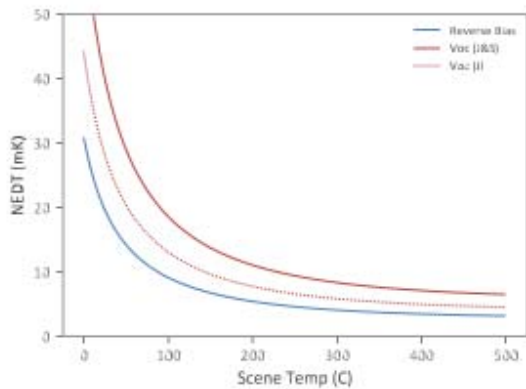 - This is due to the fact that NEDT uses a temperature (signal) differential by definition.

Approved for public release; distribution is unlimited.

Performance Equalizer: Integration Time and Dynamic Range

- We don't have infinite well capacity
  - Analog ROICs are typically limited to ~30,000 e-/μm²
  - Filled by both dark and signal currents (some NEDT numbers from previous plots not possible considering this limitation).
  - Digital pixels improve well capacity but are also more expensive, have higher power consumption, are relatively noisy and difficult to execute at small pitch and large pixel count.
- V_{oc} has well defined signal limits (0—V_{bi})
  - While operating temp impacts signal and noise, it doesn't significantly impact this signal limit range.
- V_{oc} ROIC design has the potential to provide long integration times, even at high operating temperature.
- V_{oc} ROIC design also has the potential to provide high dynamic range, as the V_{oc} signal compresses near V_{bi}.

Don't want this to be a materials problem, so what can be achieved using today's SOA SLS material?

NEDT Comparison

Parameters

Det Temp: 150 K	Scene Temp: 300 K
QE: .7	t_{int}: 15 ms (or ½ well)
j_d: 10xR07	f/#: 1
r_{sh}: ∞ Ω	Pixel Pitch: 15 μm
λ_c: 5 μm	n: 1
e_{well} density: 30,000 e-/μm²	
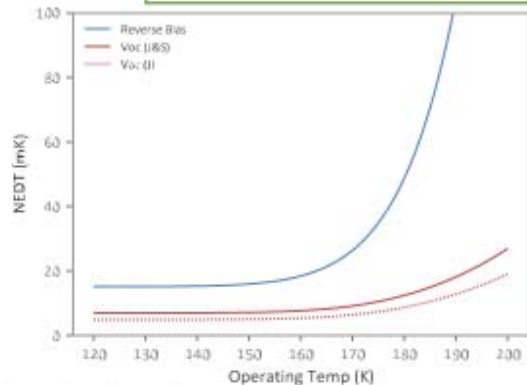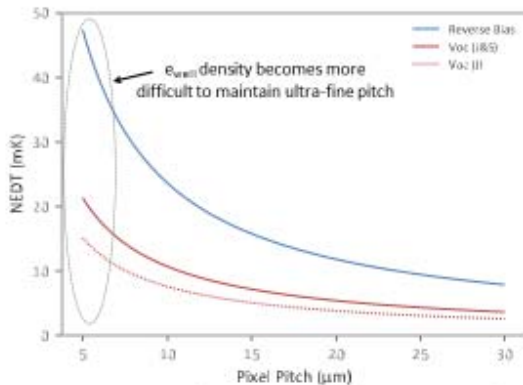
V_{oc} mode outperforms reverse bias photodiodes when integration time is limited to ½ well. **No** material development required to prove the concept.

What Can and Can't Voc Operation Provide?

- V_{oc} operation doesn't provide an inherent NEDT advantage relative to reverse bias (regardless of pitch or photon flux)
  - Despite the fact that signal doesn't change with size, noise scales to compensate
- V_{oc} operation does provide potential to integrate signal longer at higher operating temp and smaller pitch (leading to improved NEDT)
  - e_{well} density is difficult to maintain at ultra-fine pitch
  - V_{oc} signal has well defined limits that is relatively independent of operating temperature
- V_{oc} operation does provide potential for high dynamic range
  - Due to V_{oc} limited between $(0 - V_{bi})$

Conclusions

- We can reasonably model the noise characteristics at V_{oc}
  - Shot noise should likely be considered, but more measurements are required
- NEDT is a more straightforward metric to analyze V_{oc} operation
- V_{oc} mode offers no inherent NEDT advantage to a reverse bias photodiode (all things equal)
- V_{oc} mode should have a real-world NEDT advantage if we can leverage integration time (which is severely limited for a reverse bias photodiode at high operating temp).
  - No material development necessary
  - This analysis didn't require multiple diodes in series (more analysis required here)
  - Digital pixel is another approach to solving this issue, but has a host of other issues, particularly at fine pitch and high pixel count.
- e_{well} density is difficult to maintain at ultra-fine pitch, so V_{oc} mode could have advantages in this regime by leveraging integration time again
- V_{oc} mode could also have potential dynamic range advantages due to the natural signal compression near V_{bi} (high-injection models should be developed to asses this)
- Expected challenges include:
  - Optimizing the unit cell design to maximize performance (must be detector limited, not ROIC)
  - Nonuniformity correction of a nonlinear signal chain

LIST OF SYMBOLS, ABBREVIATIONS, AND ACRONYMS

ACRONYM	DESCRIPTION
AC	alternating current
ADC	analog to digital converter
AFRL	Air Force Research Laboratory
C_{INT}	integration capacitor
CIS	CMOS Image Sensor
CMOS	complementary metal oxide semiconductor
DARPA	Defense Advanced Research Projects Agency
DC	direct current
FET	field effect transistor
FFT	Fast Fourier Transform
FPA	focal plane array
HOT	high operating temperatures
ICP	interband cascade photodetector
MIM	metal-insulator-metal
MWIR	mid-wave infrared
NEP	noise equivalent power
NET	noise equivalent temperature
o.o.m.	orders of magnitude
OSU	Ohio State University
PD	photodetector
RMS	root mean square
ROIC	readout integrated circuit
SNR	signal-to-noise ratio
TIA	trans-impedance amplifier
V_{OC}	open circuit voltage
VocP	Open Circuit Voltage Photodetector